Volume 18
Number 33
7 September 2022
Pages 6141–6292

Soft Matter

rsc.li/soft-matter-journal

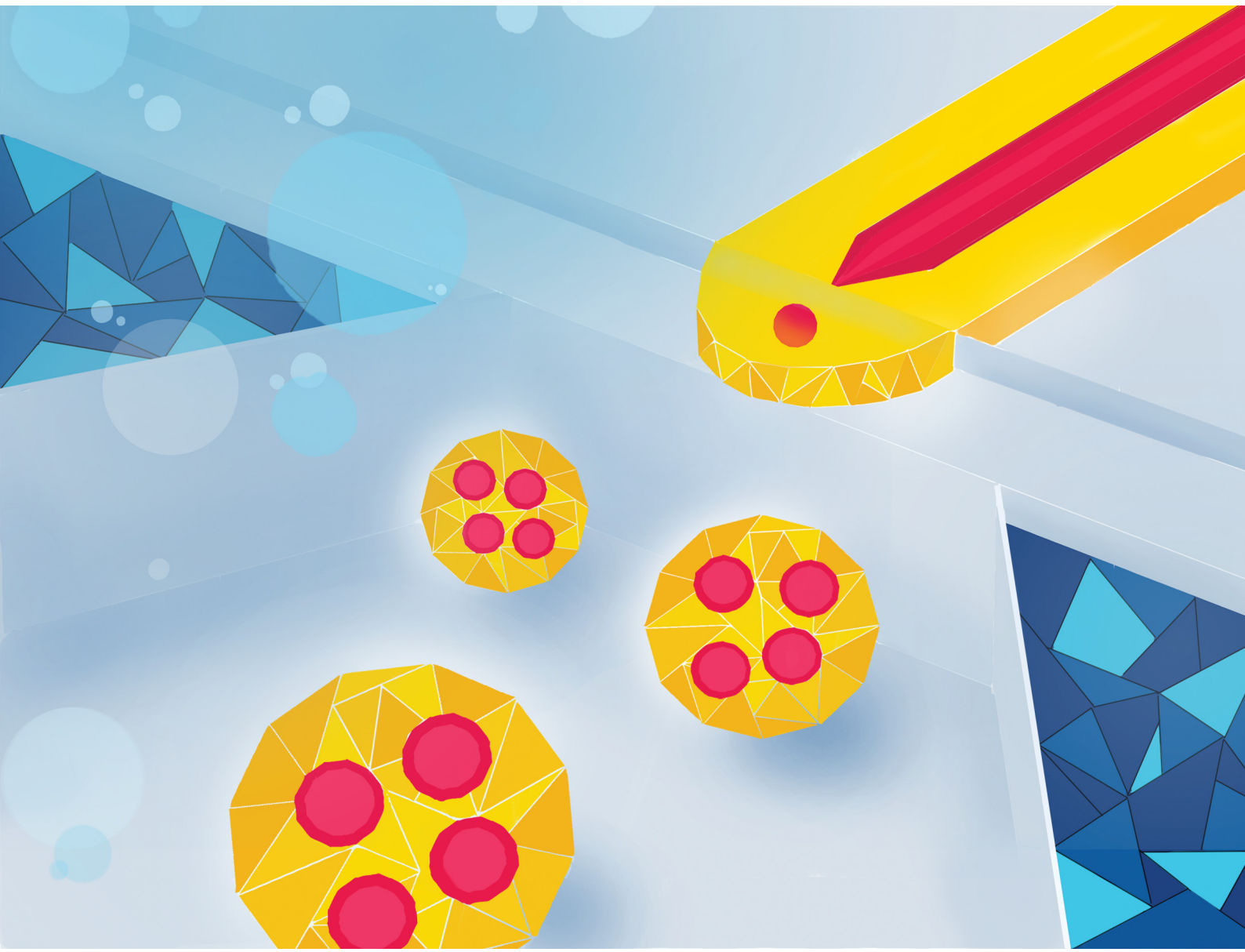

ISSN 1744-6848

ROYAL SOCIETY OF CHEMISTRY

PAPER
Ladislav Derzsi, Jan Guzowski *et al.*
A double-step emulsification device for direct generation of double emulsions

Soft Matter

PAPER

View Article Online
View Journal | View Issue

Cite this: *Soft Matter*, 2022, **18**, 6157

A double-step emulsification device for direct generation of double emulsions†

Yu-Kai Lai, [ab] Adam S. Opalski, [a] Piotr Garstecki, [a] Ladislav Derzsi *[a] and Jan Guzowski *[a]

In microfluidic step emulsification, the size of droplets generated in the dripping regime is predominantly determined by the nozzle's height and only weakly depends on the applied flow rates or liquid properties. While the generation of monodisperse emulsions at high throughput using step emulsifiers has been well established, the generation of double emulsions, *i.e.*, liquid core–shell structures, is still challenging. Here, we demonstrate a novel double-step emulsification method for the direct generation of multi-core double-emulsions and provide a predictive model for the number of cores. While the mechanism of the formation of the core droplets or empty shell droplets follows the well-established scenario of simple step emulsification, the formation of double-emulsion droplets is strongly affected by the presence of the cores. Passing of the cores through the narrowing neck of the shell postpones shell pinch-off. In particular, we demonstrate that our system can be used for the generation of arbitrary large, tightly packed droplet clusters consisting of a controllable number of droplets. Finally, we discuss the options of upscaling the system for high-throughput generation of tailored double emulsions.

Received 12th March 2022,
Accepted 1st June 2022

DOI: 10.1039/d2sm00327a

rsc.li/soft-matter-journal

1 Introduction

Double-emulsions consist of droplets encapsulating smaller immiscible droplets. In particular, water-in-oil-in-water (W/O/W) double emulsions find a wide range of applications in multiple fields of industry, including food,[1] cosmetic, and pharmaceutical products.[2] Controlling the structure of double-emulsion droplets is crucial for their use; many applications require a single core with a thin shell for encapsulation and culturing of cells in core droplets which then provides optimal nutrient and waste exchange with the external environment,[3,4] while droplets with multiple cores attract interest as vehicles for material engineering[5] and chemical communication,[6] or as smart capsules.[7] By polymerizing the core droplet in single-core structures, monodisperse solid beads with tunable properties can be rapidly prepared.[8]

Traditionally double emulsions are generated by bulk methods such as high-shear mixing or sonication.[9] The process has to be optimized to avoid unwanted single emulsions, but even then it yields polydisperse double emulsion droplets with little control over the internal structure.[10] Droplet microfluidics provides an attractive alternative as it offers a precise control over the size and number of core and shell droplets.[11] There are shear-driven microfluidic emulsification methods that produce double emulsions with the size of the core and the shell as well as the number of the cores being adjustable. Various geometries have been demonstrated for this purpose, such as double flow-focusing channels,[12–16] serial T-junctions[17,18] and nested circular capillaries.[19–25] All these methods offer good control over the size and structure of the double droplets, but the droplet generators are difficult to efficiently parallelize as the size of the droplets generated in these geometries is sensitive to even small changes in the applied flow rates.[26,27]

A promising approach to overcome this limitation is the so-called step emulsification which is characterized by a much weaker dependence of the size of the droplets on the applied flow rates.[28,29] Step emulsification takes advantage of capillary pressure imbalance as a liquid finger confined in a shallow channel enters a deep reservoir. The sudden release of confinement leads to a rapid expansion of the liquid fingertip. The decreasing Laplace pressure in a forming droplet pulls more liquid from the confined area resulting in the formation of a neck and ultimately the droplet pinch-off.[30] At sufficiently low capillary numbers the process depends only on the geometry of the nozzle and not, in particular, on the applied flow rates or viscosities or the surface tension.[31–35] The critical capillary number below which such a dripping mode is stable[36] depends on the applied width-to-height ratio of the microchannel.[37,38] Since the robust emulsification mechanism is hard-wired into

[a] *Institute of Physical Chemistry, Polish Academy of Sciences, Warsaw, Poland. E-mail: jguzowski@ichf.edu.pl*
[b] *Laboratory for MEMS Applications, IMTEK – Department of Microsystems Engineering, University of Freiburg, Georges-Koehler-Allee 103, 79110 Freiburg, Germany*

† Electronic supplementary information (ESI) available. See DOI: https://doi.org/10.1039/d2sm00327a

the geometry of the device, step emulsification is considered a suitable method for up-scaling of droplet generation by parallelizing the droplet generating units.[31–33,39–42] It is worth mentioning that in a majority of applications the continuous phase does not require precise flow control and in many cases it is even at rest. In high-throughput applications the generated droplets need to be carried away from the step in order to avoid droplet crowding.[31–33,39,40] This can be achieved by exploiting the flow of the continuous phase,[32,39,40] separation based on density difference[42,43] or their combination.[44]

Generation of double-emulsions using step emulsification is possible but much more challenging. To date the only approach to produce double emulsion droplets in microfluidic step-height geometries relies on the use of so-called tandem systems, composed of two chips connected *via* tubing,[45,46] where a monodisperse emulsion generated in the first chip is re-injected into the second chip for re-emulsification. Tandem emulsification has also been demonstrated in a PDMS device by bonding two step emulsifiers on top of each other.[47] However, the transfer of droplets between the independent emulsifiers increases the chance of core droplet coalescence due to their collisions[48] and, in general, de-synchronizes core- and shell-droplet generators which may impact core-number distribution in the final double-emulsion drops.

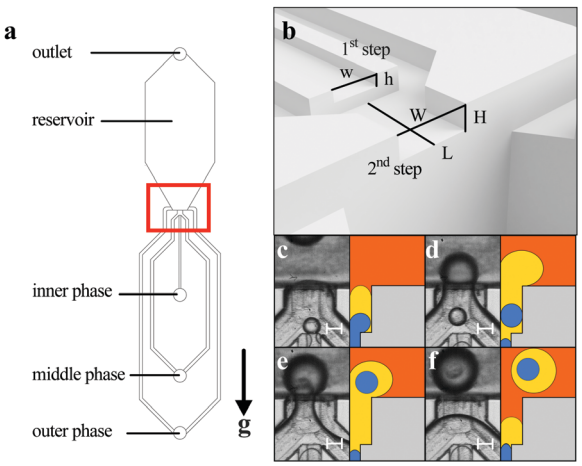

Fig. 1 (a) General layout of the microfluidic network employed in the experiments. The red box indicates the double-step geometry; the *g* direction indicates gravity. (b) 3D rendering of the geometry. (c)–(e) Experimental images and cross-sectional sketches illustrating the formation of double emulsion droplets. Scale bar: 100 μm.

Here, for the first time, we demonstrate a double-step emulsification method which allows for the direct (non-tandem) generation of double emulsion droplets with a tunable internal structure. We propose a geometry consisting of two consecutive steps, where the core droplets formed in the first step are directly encapsulated by the shell phase in the consecutive step (see Fig. 1). The process results in the generation of double-emulsion drops with multiple cores in a single shell. We demonstrate that tuning the flow rates of the two dispersed phases allows for control over the number and size of the liquid cores in double-emulsion droplets. In particular, we demonstrate the generation of drops with a large number of cores, $N \sim 20$, and rationalize the dependence of N on the core volume fraction ϕ upon ϕ approaching the close-packing limit, a regime not investigated in previous studies. Our results may help in engineering high-throughput systems for passive generation of monodisperse double emulsions with well controlled structures.

2 Materials and methods

2.1 Liquids

We used three immiscible liquid phases to generate W/O/O double emulsions. As the outer phase we used FC-40 (3 M,USA) with 1 wt% of PFPE-PEG-PFPE surfactant (Chemipan, Poland), as the middle phase we used *n*-hexadecane with 2 wt% Span 80 (Sigma-Aldrich, Germany) or its mixture with silicone oil, AP 100 (Sigma-Aldrich, Germany) (0–70% w/w) (see Table 1), and as the core phase we used distilled water with dye (Congo red). The role of a surfactant (SPAN 80) in the silicone oil/hexadecane mixture was to stabilize the aqueous droplets against coalescence. To overcome the problem of wetting the channel walls by the dispersed middle- and core phases we rendered the channel walls fluorophilic by applying the commercial fluorinated coating Novec 1720 (3 M, USA).

2.2 Microfluidic device and experiment

Experiments were carried out in devices made of either polycarbonate (PC) or poly(dimethylsiloxane) (PDMS). A network of microfluidic channels was milled in a polycarbonate plate using a CNC milling machine (Ergwind, Poland) and either bonded to another PC plate (to form a PC device) or used as a template for the fabrication of a PDMS master which allowed the fabrication of multiple replicas of the device. Channel dimensions were measured using an optical profilometer (CountourGT-K, Bruker, USA). To fabricate the master, PDMS

Table 1 The list of liquids employed in the experiments together with their basic properties. Viscosity was measured using a rotational rheometer (Malvern Panalytical GmbH, Germany). Interfacial tension was measured using the pendant drop method

Phase	Liquids	Case	ρ [g cm^3]	η [mPa s]	γ_{water} [mN m^{-1}]	$\gamma_{FC\text{-}40}$ [mN m^{-1}]
Inner phase	Distilled water with congo red	—	0.997	0.829 ± 0.023	—	—
	Hexadecane 2% w/w Span 80	A	0.770	2.999 ± 0.009	4.56 ± 0.10	5.80 ± 0.14
Middle phase	Hexadecane/AP 100/Span 80 (48 : 50 : 2 w/w)	B	0.908	8.653 ± 0.043	3.85 ± 0.02	5.88 ± 0.03
	Hexadecane/AP 100/Span 80 (28 : 70 : 2 w/w)	C	0.963	14.381 ± 0.001	2.60 ± 0.04	5.77 ± 0.09
Outer phase	FC-40 with 1% PFPE-PEG-PFPE	—	1.855	3.935 ± 0.013	—	—

(10 : 1 w/w elastomer and cross-linker) was poured onto a PC plate with milled channels, baked for an hour at 75 °C and peeled off. The mold was silanized for 3 hours at 20 mbar with tridecafluoro(-1,1,2,2,-tetrahydrooctyl)-1-trichlorosilane (Alfa Aesar, Germany). Such a mold was then filled with PDMS and baked for an hour at 75 °C, ad then the cured PDMS was peeled off. After punching the holes with a needle the PDMS cast was bound to glass using oxygen plasma treatment. Surface modification was achieved by filling the channel with Novec 1720 (3 M, USA) and baking the device at 130 °C for 30 minutes. We note that, after micromilling, the walls of the channels remained rough, with roughness of the order of 5 μm (see Fig. S2, ESI†). Such surface roughness is actually known to improve the effectiveness of the fluorophilic coating of polycarbonate with Novec 1720.[28] In order to avoid even partial wetting of channel walls by the dispersed phases, first we filled our devices with the outer phase and only then introduced the to-be dispersed phases.

In all microfluidic experiments neMESYS syringe pumps (Cetoni, Germany) were used to inject liquids at flow rates ranging from 0.1 μl min^{-1} to 15 μl min^{-1}. Droplet formation on-chip was recorded using a monochrome fast camera (1024PCI, K100, Photron, Japan). The droplet diameters were measured either manually using ImageJ or automatically with dedicated software.[49] The droplet volume and diameter in the confined geometry were calculated assuming a filled-torus morphology, which has been shown to accurately describe the shape of a droplet flattened by the walls of a microchannel (see Fig. S1, ESI†).

3 Results

3.1 Microfluidic devices

The geometry of the device we used for emulsification is presented in Fig. 1a and b. The key features are the heights/depths of the inlet channel and the plateau (h = 42 μm, H = 98 μm, respectively), their widths (w = 162 μm and W = 345 μm, respectively), and the length of the plateau (L = 280 μm). According to previous research,[37,41] the diameter of the generated droplets at either step was expected to range from 3 to 4 times the height of the preceding channel, *i.e.*, 3h–4h for core droplets and 3H–4H for shell droplets, and we considered this fact while designing our device. Since in most of the applications double-emulsion drops with thin shells are preferred, the ratio H/h should be kept possibly small. However, when $H/h < 2$, the size of the droplets generated at the first step depends not only on h but also on H.[30] To ensure that both steps feature simple step emulsification, we keep $H/h \geq 2$. Here, we used the device with H/h ratio equal 2.3. Note that the dimensions of the outer channels supplying the external phase do not affect droplet formation (Fig. 1a). These channels serve only to deliver the outer phase to the reservoir prior to the experiment but do not operate during the experiment.

3.2 Dimensionless parameters

In order to study the dynamics of droplet formation, we characterized our system by several variables such as the flow rates of the inner and middle phases, Q_i and Q_m, respectively. We denote the viscosities of the inner, middle, and outer liquid phases as η_i, η_m, and η_o, the densities as ρ_i, ρ_m, and ρ_o, respectively, and the relevant interfacial tensions as $\gamma_{i,m}$, and $\gamma_{m,o}$. We also introduce the core droplet volume fraction defined as $\phi = Q_i/(Q_i + Q_m)$.

We further introduce the capillary numbers $Ca_i = \eta_i U_i/\gamma_{i,m}$ and $Ca_m = \eta_m U_m/\gamma_{m,o}$, of the inner and middle phases, respectively, with the linear velocities $U_i = Q_i/(wh)$ and $U_m = Q_m/(WH)$ and the Bond numbers, $Bo_i = (\rho_i - \rho_m)gD_i^2/\gamma_{i,m}$ and $Bo_m = (\rho_o - \rho_m)gD_m^2/\gamma_{m,o}$ where D_i and D_m are the diameters of the droplets of the inner phase (in the middle phase) and middle phase (in the outer phase; here, without cores in the middle phase). The diameters were measured by image analysis (see Fig. S2, ESI†). We found that Bo_i was of the order 10^{-3} meaning that the effects of gravity were negligible in the generation of core droplets. In contrast, Bo_m was in the range 10^{-1}–10^{0} depending on the actual size of the droplets. In any case, we expect that, except for very large double-emulsion drops, gravity also had a minor impact on drop formation (we discuss the validity of the model in the Discussion section).

3.3 Decoupling shell and core droplet formation

To compare the operation of our double-step droplet generator with the operation of standard single-step generators described previously in the literature, we first studied the formation of single droplets at the first or the second step with only two liquid phases.

First, we removed the outer liquid (FC-40) from the system and blocked the inlet port of the outer phase. Before injecting the inner (core) phase, we waited until the shell phase completely filled the reservoir, and then, keeping the shell phase flowing, we turned on the flow of the inner phase. We recorded the droplet generation and measured the diameter of core droplets D_i formed in the first step as a function of the flow rates of the inner and middle phases (see Fig. 2). We observed a stable generation of monodisperse inner phase droplets up to Q_i = 5 μl min^{-1} (corresponding to $Ca_i^* \simeq 0.0024$), above which transition to the jetting regime (also known as the balloon regime[35])

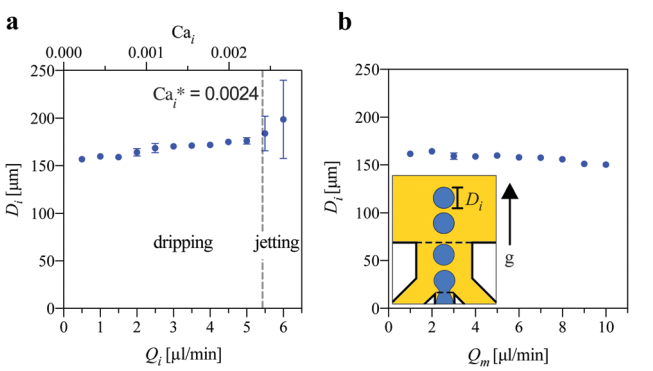

Fig. 2 The diameter of the core droplets (D_i) generated in the first step inside the middle phase without the supply of the outer phase as a function of the flow rate of (a) the inner phase Q_i (at Q_m = 5 μl min^{-1}) and (b) the middle phase Q_m with Q_i held constant. (Q_i = 1 μl min^{-1}). Sub-panel: a schematic representation of the experimental setup.

took place. The measured diameter of the inner phase droplets, D_i increased by approximately 12% in this regime which is typical for step emulsifiers.[30,32,37,41] We note that, due to the density of the droplet phase being higher than that of the external phase, during these experiments the microfluidic device had to be flipped, with the nozzle facing upwards, so we could take advantage of buoyancy to remove the generated droplets from the nozzle. However, this proved not to be always sufficient, particularly in cases B and C (see Table 1), where the density difference between the oil and aqueous phases was small. Therefore, in this series of experiments we let the middle phase liquid flow at Q_m, which we changed between 1 and 10 μm min^{-1}. We plotted the diameter of the generated core droplets as the function of Q_m and Q_i, and found that the flow of the middle phase did not affect the formation of core droplets. For a fixed Q_i we observed only a minor non-systematic variation of the droplet size D_i which did not exceed 7% (Fig. 2b).

Next, we measured the diameter of empty shell droplets D_m, *i.e.* droplets of the middle phase formed in the second step in the absence of the inner phase. Droplets broke off into the reservoir filled with the outer phase liquid (FC-40), which was at rest and the formed droplets were carried away from the step by buoyancy. For all viscosities η_m we observed a slight increase of the droplet diameter D_m with the applied flow rate Q_m until the transition to the jetting regime at around $Ca_m = Ca_m^* \sim 0.003$ (Fig. 3b).

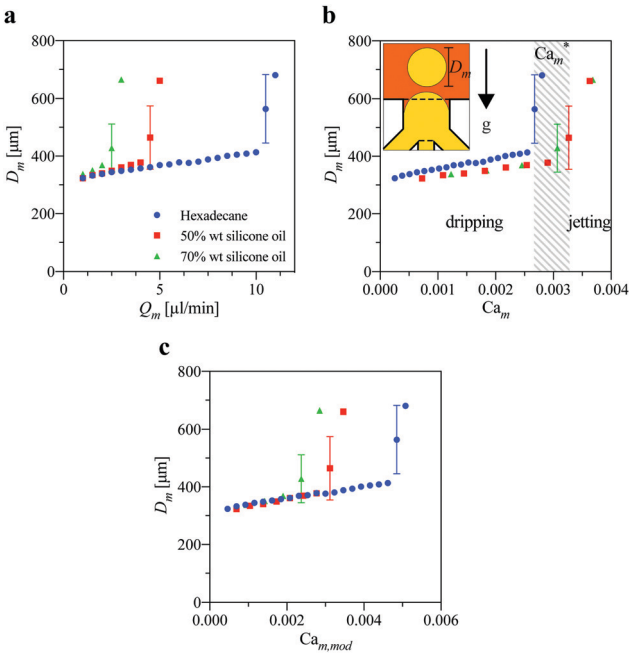

Fig. 3 (a) Diameter of the shell droplet (D_m) generated in the second step as a function of the flow rate Q_m of the middle phase for various types of the middle phase with the inner phase turned off, $Q_i = 0$. (b and c) The same data plotted as a function of (b) the capillary number Ca_m and (c) the modified capillary number $Ca_{m,mod}$. Sub-panel: a schematic representation of the experimental setup.

As we expected, in the case of the core droplets and the empty shell droplets, the mechanism of droplet formation and the dripping to jetting transition follow the classic scenario of the simple step emulsification well-described in the literature. By the "classic scenario" we mean the situation in which the dispersed phase pushed through a shallow and wide rectangular microchannel enters a deep reservoir, and the sudden release of confinement compels the tip of the liquid finger to rapidly round off in order to minimize the area of the liquid–liquid interface. The resulting pressure drop in the microchannel leads to the formation of a neck which eventually breaks. Such interfacial-tension driven mechanism of droplet breakup results in the size of droplets being predominantly set by the geometry of the device, in particular the height of the shallow inlet channel. Empirical studies[37,41] showed that in order to precisely predict the size of the generated droplets (Fig. 3b) the viscosity of the continuous phase also needs to be taken into account. Accordingly, we also investigated the dependence of the size of the droplets D_m formed at the second step on the modified capillary number defined as $Ca_{m,mod} := (\eta_o + \alpha'\eta_m)U_m/\gamma_{m,o}$ with a numerical constant α' depending on the geometry of the device. We found that, within the dripping regime, and with the constant adjusted to $\alpha' = 0.5$, D_m was determined solely by $Ca_{m,mod}$ (Fig. 3c), a consideration that remains in line with the previous studies.[37] In the next section, we present and discuss new results considering the generation of double-emulsion droplets at the double-step geometry.

3.4 Formation of double emulsion droplets

We now consider the case in which the flows of both the inner and middle phases are turned on, and the reservoir is filled with the third, outer phase liquid (Fig. 4). We observe that the presence of the third liquid phase in the outlet reservoir has little effect on the formation of the core droplets in the first step. We also observe only a minor variation of the core diameter D_i with Q_i (Fig. 4a) and Q_m or upon changing the type of the middle phase.

The most significant change can be observed in the formation of the middle phase droplets in the second step as the growing droplet is filled not only by the middle phase but also by the core droplets. We observed a significant increase in the diameter D_{DE} of the double emulsion (DE) droplets as compared to the diameter of the empty shell droplets observed earlier. The increase in the diameter can be associated with postponed pinch-off which results from the core droplets continuously passing through the plateau between the two steps towards the forming shell droplet, recurringly expanding the neck. Previously, it was reported[37,38] that the increasing flow rate of the disperse phase postpones droplet break-up at the step as the dynamic pressure within the neck increases, thus stabilizing the neck. Here, the situation is similar with the difference that the dynamic pressure in the thinning neck is increased periodically every time a core droplet passes through it. The periodic oscillation of the width of the neck is shown in Fig. 5b. Building on previous works describing the dynamics of simple step emulsification and combining it with our

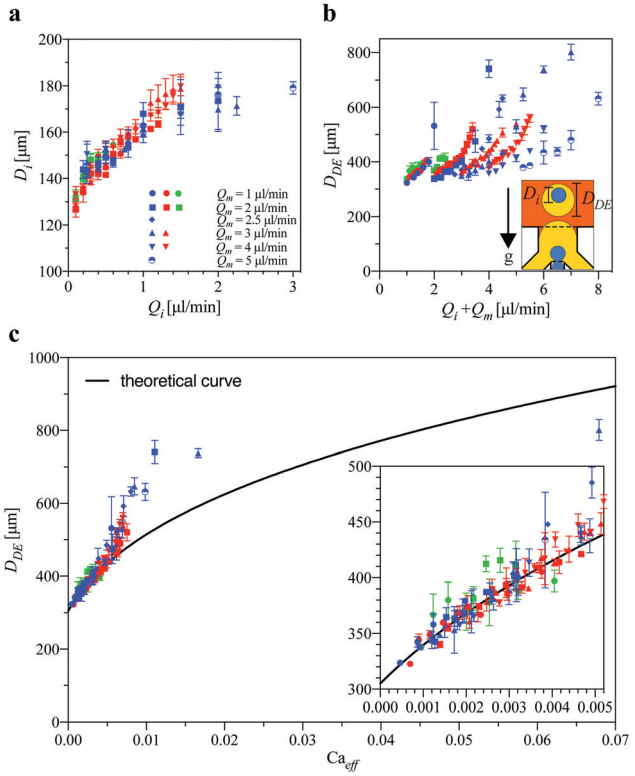

Fig. 4 (a) The diameter D_i of the core droplets as a function of Q_i for various Q_m and various types of the middle phase. (b) The corresponding diameter D_{DE} of the double-emulsion drops as a function of the net flow rate $Q_i + Q_m$. Subpanel: a schematic representation of the experimental setup. (c) D_{DE} as a function of the effective capillary number Ca_{eff}. The solid line is the theoretical prediction (eqn (15) with β = 380, D_0 = 305 μm). Inset: $Ca_{eff} \in$ [0, 0.0052]. Symbols in the blue/red/green color correspond to middle phase fluids A, B, and C.

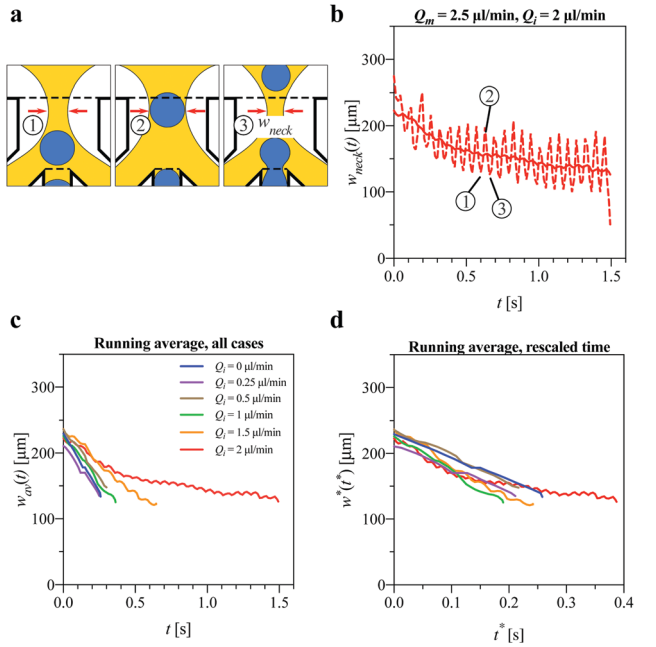

Fig. 5 (a) A scheme showing the widening of the neck upon core passing through it; black dashed line indicates the steps. The outer phase is not colored for visibility. (b) Dashed line: time evolution of the neck width $w_{neck}(t)$ of the shell phase at Q_i = 1 μl min^{-1} and Q_m = 2.5 μl min^{-1}. Solid line: time evolution of the time-averaged neck width $w_{av}(t)$ (see eqn (11)) obtained as a running average of $w_{neck}(t)$ with the averaging window T = 0.3 s (roughly 3 x the period of oscillations). Time t = 0 marks the moment when the tip of the dispersed phase reaches the edge of the step (t_s). (c) The running average $w_{av}(t)$ for various flow rates of the inner phase Q_i at Q_m = 2.5 μl min^{-1}. (d) Data from panels (c) plotted *versus* the rescaled time $t^* = t\,(1 - \phi/\phi_0)$, according to eqn (13) with ϕ_0 = 0.6.

experimental observations, in the following paragraph we provide a quantitative model of the above described 'postponed dripping'. In particular, we predict the diameter of the DE droplets and the number of the encapsulated cores as a function of the applied flow rates in the whole regime of available volume fractions.

3.5 Theoretical model of postponed dripping

Necking time $\mathscr{T}_n$. First, we consider the generation of the drops of the middle phase in the case without cores. We denote by t^* the 'stage of thinning' of the neck of the middle phase, where $t^* = 0$ corresponds to the formation of the neck and $t^* = \tau_n$ to neck breakup. More precisely, after Crestel *et al.*,[41] we define $\tau_n = t_b - t_s$, where t_b is the time of neck breakup and t_s is the time of neck formation, *i.e.*, the moment in which the meniscus passes the edge of the step.

Now, in the case with the cores, our experimental observations (Fig. 5b) suggest that the neck temporarily widens each time a core passes through it. We assume that such widening proportionally postpones neck breakup by a time interval Δt_i corresponding to the transit of the core through the thinnest part of the neck. Accordingly, the actual time $\mathscr{T}_n$ of thinning of the neck in the case with the cores can be calculated as

$$\mathscr{T}_n = \tau_n + N\Delta t_i = \tau_n\left(1 + \frac{\Delta t_i}{\Delta t^*}\right) \quad (1)$$

where Δt^* is the time that passes between one core leaving and the next core entering the neck. We note that the time of generation of a single core T_i can be written as $T_i = \Delta t^* + \Delta t_i$, from which

$$\Delta t^* = T_i - \Delta t_i. \quad (2)$$

From eqn (1) and (2) we obtain

$$\mathscr{T}_n = \tau_n\left(1 + \frac{\Delta t_i}{T_i - \Delta t_i}\right) = \frac{\tau_n}{1 - \Delta t_i/T_i}. \quad (3)$$

The transit time Δt_i can be approximated as

$$\Delta t_i = D_i'/U_{neck}, \quad (4)$$

where U_{neck} is the core velocity inside the neck and D_i' is the apparent diameter of the core droplets flattened by the upper and lower wall at the plateau between the steps. We will use the approximation $U_{neck} = (Q_i + Q_m)/S_{neck}$ where S_{neck} is the average area of the neck cross-section over the time at which the cores transit the neck, that is

$$S_{neck} = Hw_0, \quad (5)$$

where

$$w_0 = \langle w_{\mathrm{neck}}(t)\rangle_{[t1,tN]}. \quad (6)$$

Here, $w_{\mathrm{neck}}(t)$ is the actual fluctuating neck width, $\langle\ldots\rangle_T$ means averaging over the time interval T and $[t_1, t_N]$ is the time interval between the first and the last (N-th) core transit.

Since $T_i = V_i/Q_i$, where V_i is the volume of a single core and $\Delta t_i = D_i' S_{\mathrm{neck}}/(Q_i + Q_m)$, we then substitute Δt_i and T_i in eqn (3) and obtain

$$\mathscr{T}_n = \frac{\tau_n}{1 - \frac{D_i' S_{\mathrm{neck}}}{V_i}\frac{Q_i}{Q_i + Q_m}}. \quad (7)$$

We can rewrite

$$\mathscr{T}_n = \frac{\tau_n}{1 - \phi_0^{-1}\phi} = \tau_n \psi_0(\phi), \quad (8)$$

where $\phi = Q_i/(Q_i + Q_m)$ is the volume fraction and

$$\psi_0(\phi) = \frac{1}{1 - \phi_0^{-1}\phi}, \quad (9)$$

is the necking-time scaling function and

$$\phi_0 = \frac{V_i}{D_i' S_{\mathrm{neck}}} \quad (10)$$

is the critical volume fraction corresponding to the transition to the 'no pinch-off' regime, *i.e.*, the formation of an indefinitely growing shell ('$N = \infty$'). Since V_i, D_i', and S_{neck} are nearly independent of the applied flow rates, ϕ_0 can be treated as a constant depending only on the geometry of the junction. Actually, ϕ_0 can be acquired directly from the experiment *via* measuring the average values V_i, D_i', S_{neck}.

Next, we turn to the evolution of the neck width $w_{\mathrm{neck}}(t)$ from the moment of neck formation at $t = 0$ to its breakup at $t = \mathscr{T}_n$. In the experiment we observe that $w(t)$ consists of fluctuations around a slowly varying envelope $w_{\mathrm{av}}(t)$, where

$$w_{\mathrm{av}}(t) = \langle w_{\mathrm{neck}}(t')\rangle_{[t,t+T]}, \quad (11)$$

where T is an averaging interval larger than the oscillation period T_i, *i.e.*, such that $T > T_i$. We assume that $w_{\mathrm{av}}(t)$ is approximately equal to the non-fluctuating width of the neck w^* in the case without the cores at the corresponding stage of thinning t^*, *i.e.*, that

$$w_{\mathrm{av}}(t) = w^*(t^*), \quad (12)$$

where in analogy to eqn (1) we assume that

$$t = t^*\left(1 + \frac{\Delta t_i}{\Delta t^*}\right) = t^*\psi_0(\phi). \quad (13)$$

We can verify the scaling formula in eqn (12) using the actual experimental data $w_{\mathrm{neck}}(t)$ (Fig. 5). To this end, we first determine ϕ_0 using eqn (10) in which we estimate S_{neck} (eqn (5) and (6)) by taking t_1 as the first local minimum and t_N as the last local maximum of $w_{\mathrm{neck}}(t)$. *Via* averaging the data in the cases with various Q_i, at $Q_m = 2.5$ μl min^{-1} and $Q_m = 4$ μl min^{-1} (the data for $Q_m = 2.5$ μl min^{-1} are shown in Fig. 5c), we obtain $w_0 \simeq 0.17$ mm which leads to $S_{\mathrm{neck}} \simeq 0.17$ mm^2. By using image analysis we also find $D_i' \simeq 167$ μm $\pm$ 9 μm (the average apparent core diameter in the cases with $Q_i \in \{0.25, 0.5, 1.0\}$ μl min^{-1} and $Q_m \in \{2.5, 4.0\}$ μl min^{-1}) from which (*via* applying the nodoid model, see the ESI†) we find $V_i \simeq 1.68 \pm 0.09$ nl. Those values eventually lead to the estimation of $\phi_0 \simeq 0.60 \pm 0.03$ which allows testing the scaling proposed in eqn (13). In fact, we find that the experimental data for w_{neck} plotted for various Q_i and Q_m values against the rescaled time $t^*/\psi_0(\phi)$ (eqn (13)) with $\phi_0 = 0.6$ tend to collapse onto a single master envelope (Fig. 5d).

Drop size D_{DE} and the effective capillary number Ca_{eff}. Adopting the reasoning proposed previously for simple step emulsification[41] we assume that the volume V_{DE} of a double-emulsion drop generated at a step can be expressed as a sum of two contributions: (i) the minimum drop volume V_0 set solely by the geometry of the device and (ii) the volume injected during the necking time $\mathscr{T}_n = \tau_n\psi_0(\phi)$. This assumption leads to

$$V_{DE} = V_0 + (Q_i + Q_m)\tau_n\psi_0(\phi). \quad (14)$$

Next, drawing from previous works considering step emulsification,[37,41] we assume $\tau_n = \frac{a}{\gamma_{m,o}}(\eta_o + \alpha\eta_m)$ where a and α are model constants (a has the dimension of length and α is non-dimensional). We also introduce the net velocity of the dispersed phases at the second step, $U_{DE} = (Q_i + Q_m)/(HW)$ which, considering that $V_{DE} = \pi D_{DE}^3/6$, allows us to rewrite eqn (14) in the form

$$D_{DE} = D_0\,(1 + \beta \mathrm{Ca}_{\mathrm{eff}})^{1/3}, \quad (15)$$

where $D_0 = (6V_0/\pi)^{1/3}$ and $\beta = aHW/V_0$ are the parameters which can be fitted directly to the data D_{DE} (Ca_{eff}), and where

$$\mathrm{Ca}_{\mathrm{eff}} = \psi_0(\phi)(\eta_o + \alpha\eta_m)U_{DE}/\gamma_{m,o} \quad (16)$$

is the effective capillary number describing the generation of double-emulsion drops accounting for the effects of packing of the cores as well as for the viscosities of both the middle and the outer phases.

In agreement with those predictions, the experimentally measured diameters of double-emulsion drops D_{DE} for various Q_i and Q_m values plotted as a function of Ca_{eff} upon adjusting $\alpha = 0.5$ and $\beta = 380$ collapse onto a master curve (Fig. 4c). Note that we find $\alpha = \alpha'$ (the latter appears in the definition of $Ca_{m,mod}$ in Section 3.3.) which confirms the consistency of our model. Further, we find that the scaling proposed in eqn (15) holds for the effective capillary numbers Ca_{eff} below approximately 5×10^{-3}. In this regime fitting of eqn (15) to the collapsed data leads to $D_0 = 305$ μm from which we also find $a = 167.5$ mm. For higher Ca_{eff} we observe that D_{DE} (Ca_{eff}) grows faster than expected, resembling the transition to jetting (see Fig. 2 and 3). Remarkably, the data for various viscosities of the middle phase η_m collapse even in the 'jetting' regime, unlike in the case of simple middle-phase dripping (*i.e.*, in the case without the cores, see Fig. 3c). However, the data collapse seems to fail at $Ca_{eff} > 0.012$ (which typically corresponds to the cases with $\phi \geq 0.5$). The outliers in this regime have D_{DE} values smaller than those expected from the master curve

which might be attributed to the faster pinch-off of very large drops, *e.g.*, due to their buoyancy (in fact, we checked that in these cases the Bond number approaches unity) or as a result of the irregularities in the feeding of the core droplets into the shell at long times.

The number *N* of encapsulated cores. Based on the above results the total number N of encapsulated cores can be calculated as $N = \phi V_{DE}/V_i$. Using eqn (14) we obtain

$$N = \frac{V_0}{V_i}\left(\phi + \frac{Q_i \psi_0(\phi)}{Q_0}\right), \tag{17}$$

where the characteristic flow rate

$$Q_0 = \frac{V_0}{\tau_n} \tag{18}$$

can be treated as a constant for a given set of fluids and the geometry of the device.

To calculate the map $N(Q_i, Q_m)$ we take the value $V_0 = \pi D_0^3/6 = 14.9$ nl (where D_0 is taken from the fit to the data $D_{DE}(Ca_{eff})$ based on eqn (15) as discussed above) and estimate τ_n by extrapolating the experimentally measured $w_{neck}(t)$ towards $w_{neck} = 0$ in the cases with the inner phase switched off, $Q_i = 0$ μl min^{-1}, $Q_m = \{2.5; 4\}$ μl min^{-1} (we take the average of the two measurements); we obtain $\tau_n \simeq 0.22$ s. With these values we find good agreement between eqn (17) (Fig. 6b) and the experimentally measured N (Fig. 6a) without any additional fitting parameters. We note, in particular, that the theoretical formula (eqn (17)) predicts $N = \infty$ for $\phi \geq \phi_0$ (black region in Fig. 6b). In the experiment we indeed observe no double-emulsion drop pinch-off in this regime (Fig. 6a) but rather the formation of an indefinitely growing double-emulsion 'tongue'.

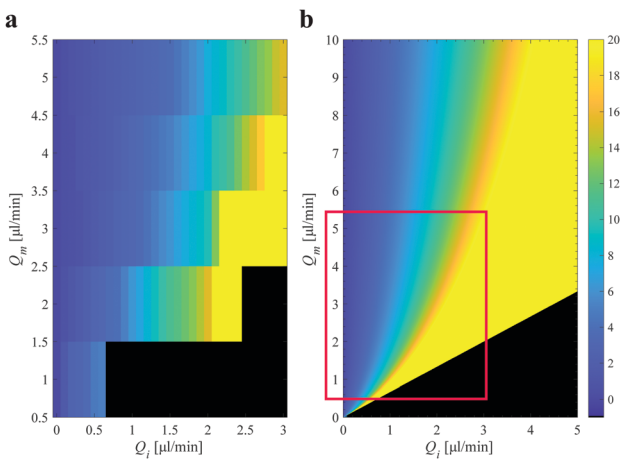

Fig. 6 (a) Experimental measurements: the heat map representing the number N of core droplets in the double-emulsion drops generated for various Q_i and Q_m using the middle fluid Case A. The colors indicate interpolated experimental data. The actual data points N were collected at $Q_i \in [0, 3]$ and $Q_m \in [0.5, 5.5]$ μl min^{-1}, at intervals 0.5 and 1.0 μl min^{-1}, respectively, in each case as an average of 11 generated double-emulsion drops. The black region corresponds to $N > 20$. (b) Theoretical prediction of the proposed model (eqn (17) with $V_0 = 14.9$ nl, $V_i = 1.68$ nl, $Q_0 = 4.1$ μl min^{-1}, reflecting typical experimental conditions). The black region corresponds to a diverging N ('$N = \infty$'). The red box indicates the experimental regime considered in panel (a).

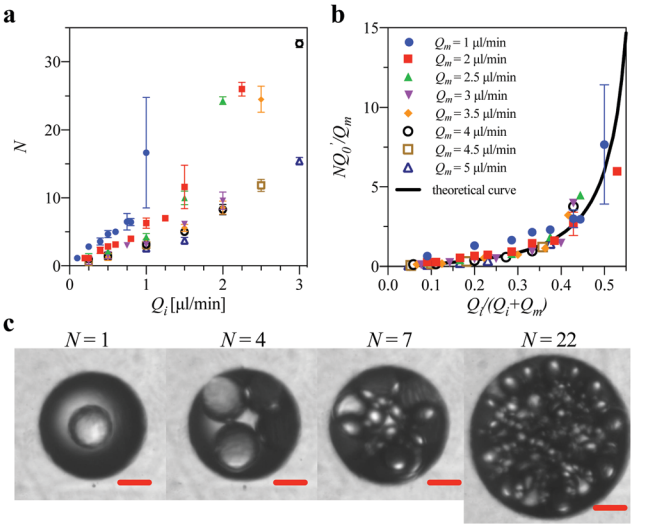

Fig. 7 (a) The number N of cores in the double-emulsion drops as a function of Q_i for various Q_m. (b) N rescaled with Q_m/Q_0' as a function of the volume fraction $\phi = Q_m/(Q_i + Q_m)$. The solid line is the theoretical prediction (eqn (21) with $Q_0' = 0.46$ μl min^{-1} reflecting the typical experimental conditions). (c) Images of the DE droplets with various numbers of core droplets. Scale bar: 100 μm.

Furthermore, we note that for large volume fractions ϕ, *i.e.*, for ϕ approaching the threshold ϕ_0, the scaling function $\psi(\phi)$ diverges, whereas Q_i/Q_0 remains around or less than unity ($Q_i \in [1, 3]$ μl min^{-1} and $Q_0 \simeq 4.1$ μl min^{-1}), which means that the first term in eqn (17) can be neglected. In such a case we obtain:

$$N = \frac{Q_i}{Q_0'} \times \psi_0(\phi), \tag{19}$$

where

$$Q_0' = \frac{V_i}{\tau_n}. \tag{20}$$

Dividing eqn (19) by Q_m and multiplying by Q_0' we obtain

$$\frac{NQ_0'}{Q_m} = \frac{\phi}{(1-\phi)} \times \psi_0(\phi), \tag{21}$$

In particular, eqn (21) can be used to collapse the experimental data $N(Q_i)$ obtained for various Q_m values (Fig. 7a) onto a single master curve (Fig. 7b). In principle, one should expect the scaling to be valid only for sufficiently large volume fractions. Despite that, we observe reasonable collapse over nearly the entire range of applied volume fractions. We take $Q_0' = 0.46$ μl min^{-1} (eqn (20)), calculated based on the values of V_i and τ_n estimated from the experiments described above.

4 Discussion and conclusion

In this work we study the formation of double emulsion (DE) drops with one or multiple cores using a double-step emulsifier. We find the the size of the cores D_i is roughly independent of the applied flow rates Q_i and Q_m (of the core and shell

phases, respectively), whereas the size of the double-emulsion-drops D_{DE} (Fig. 4) and the number of the encapsulated cores N (Fig. 6 and 7) depend on both Q_i and Q_m. In particular, we find that N diverges upon the volume fraction of the cores $\phi = Q_i/(Q_i + Q_m)$ approaching the threshold ϕ_0 (for the studied geometry we find $\phi_0 = 0.60$), see Fig. 6a. We refer to such behavior as 'postponed dripping': in this regime close-packing of the cores postpones double-emulsion drop pinch-off. In particular, we find periodic widening of the shell neck upon cores transiting the plateau between the two steps. Based on this observation we establish a scaling function $\psi_0(\phi)$, depending parametrically on ϕ_0, which describes the effective delay in the necking time $\mathscr{T}_n$ (eqn (8)) and allows us to define the effective capillary number Ca_{eff} (eqn (16)). We further derive formulas for $D_{DE}(Ca_{eff})$ (eqn (15)) and $N(Q_i, Q_m)$ which remain in good agreement with the experimental data. In particular, we also find that (at moderate ϕ) N/Q_m is a function only of ϕ (eqn (21)).

We note that our model is based on the 'proportionality hypothesis' which we introduce as an empirical assumption, following the observation of similar shapes of the envelopes $w_{av}(t)$ describing the running average of the neck width *versus* time for various volume fractions (Fig. 5c and d). One possible way of justifying such an assumption is that, in step emulsification, the dynamics of neck thinning is driven predominantly by the surface tension and, in particular, that the necking time is nearly independent of the applied flow rates, a fact known from previous studies.[37,41] Accordingly, in the case without the cores, it is the shape of the neck at a given moment in time that determines the dynamics of further neck thinning. In the case with the cores, when a core enters the neck, the thinning stops, and then continues after the core leaves the neck.

While the model works remarkably well in a wide range of volume fractions ϕ, it neglects the impact of buoyancy of the DE drop on its pinch-off. We expect buoyancy to actually accelerate pinch-off which then should lead to the generation of DE drops smaller than those predicted using eqn (15) (and the number of cores N smaller than those predicted using eqn (17)). The impact of buoyancy could be expected to be particularly strong in the case of larger drops $N \sim 20$ (which are expected to occur at ϕ close to ϕ_0) for which the Bond number could approach or even exceed unity.

Furthermore, in the actual experiments the cores are not always perfectly packed, even at high ϕ, which leads to local fluctuations in the packing fraction. Since the neck thins very quickly in the time between the transit of the subsequent cores (see Fig. 5), any irregularities in the rate of feeding of the cores to the neck may result in DE drop pinch-off. Accordingly, the local fluctuations may lead to the generation of finite DE drops even for the average ϕ being at or above the threshold ϕ_0. As a consequence the generated DE drops are smaller than those predicted by the theory and slightly polydisperse. Indeed, we observe larger error bars of the measured D_{DE} for ϕ close to ϕ_0, see Fig. 7b. Here, we do not investigate the distribution of the DE drop sizes in detail. However, we have recently provided a detailed analysis of such distributions for a related system generating DE droplets *via* flow-focusing.[50]

We note that the previous studies on tandem step emulsification predominantly considered either low-ϕ regimes[45] or different step geometries which did not support the stabilization of the neck by the cores.[46] The main novelty of our work is providing the rationale behind the generation of DE drops in the high-ϕ regime[51] allowing for the controlled generation of structures with large numbers of close-packed cores ($N > 10$), *i.e.*, for the formation of soft-granular aggregates. The demonstrated microfluidic formulation of such structures is an important step towards the fabrication of mesoscale functional materials such as multi-compartment capsules or mesoporous microbeads with exciting new applications, *e.g.*, in tissue engineering.[5]

We suppose that changing the geometry by varying W or w as long as $w/h > 2.6$ and $W/H > 2.6$ would have little effect on the operation of the device since in this regime the sizes of the droplets are set predominantly by the heights of the channels (h and H).[37,38,41,52] Another parameter of interest is the ratio of the interfacial tensions of the shell and of the cores, $\gamma_{m,o}/\gamma_{i,m}$, which in our experiments was in the range [1,2]. However, if this ratio was much larger than unity, $\gamma_{m,o}/\gamma_{i,m} \gg 1$, one could expect the inner droplets to comply with the shape of the thinning neck rather than to expand the neck. In such a case, one would expect the effect of postponed dripping to be less pronounced. Accordingly, one could speculate that the critical volume fraction ϕ_0 should increase with an increase in $\gamma_{m,o}/\gamma_{i,m}$.

Considering the range of available droplet sizes, we find that, in agreement with the previous literature,[37,38,41] the core size D_i is set predominantly by the height of the supply channel h, with $D_i \sim 4h$ (see Fig. 2). It has been shown previously that step emulsification enables generation of droplets with diameters ranging from submicrons to 1000 μm.[34,42] In order to achieve DE droplets with micron-sized cores one would need to fabricate ultra-shallow channels with h in the submicron regime. Such small dimensions are outside the reach of micromilling, but could be achieved using, *e.g.*, photolithography followed by etching.[34] Considering the upper limit of the size of the clusters, we find that, as already noted, the number N of encapsulated cores tends to grow indefinitely upon ϕ approaching the threshold ϕ_0 (Fig. 7b), yet with increasing fluctuations.

Next, considering the throughput of the device, from our experimental data (Fig. 4b) it follows that the maximal available flow rates $Q_i + Q_m$ are typically of the order of several μl min^{-1} and therefore are not excessive. However, we believe that the generation of double emulsions could be upscaled *via* parallel integration of multiple double-step nozzles. The advantage of the proposed geometry would be the relatively weak dependence of the size of the generated DE drops on the applied flow rates or their fluctuations, at least for ϕ by a safe margin below the threshold ϕ_0 (here, for $\phi < 0.5$, see Fig. 7b).

In this work, as a proof of concept, we have studied the generation of water-in-oil-in-oil (W/O/O) droplets whereas many applications such as, *e.g.*, cell encapsulation, require W/O/W droplets. In order to generate W/O/W double emulsions one would need to apply selective hydrophilic/hydrophobic surface modification of the double-step geometry. Such modification

would require very precise hydrophilicity patterning. In particular, the water inlet channel and the vertical wall behind the first step would need to be modified to be hydrophobic, while the rest of the device, hydrophilic (Fig. S3, ESI†). Such selective modification is challenging (we have not attempted it in this work) which may be a limitation of our device. Anyway, we expect our quantitative considerations considering the postponed dripping regime (Section 3.5) to remain valid independent of the type of emulsion (W/O/O or W/O/W), as long as the droplets do not wet the walls of the channels.

Last but not least, the more complex geometries similar to the double-step geometry presented here, but with multiple steps, could also facilitate direct generation of multiple emulsions consisting of three or more immiscible phases, in a manner similar to the methods exploiting multiple co-axial capillaries or multiple serial flow-focusing junctions.[20,53]

Conflicts of interest

There are no conflicts to declare.

Acknowledgements

The authors thank Airit Agasty for viscosity measurements, Agnieszka Koszewska for providing samples, and Patryk Adamczuk and Karol Patyrak for the microfabrication of the devices. This publication is part of a project that received funding from the European Union's Horizon 2020 research and innovation programme under the Marie Skłodowska-Curie grant agreement No. 711859 and scientific work funded by the financial resources for science in the years 2017–2021 awarded by the Polish Ministry of Science and Higher Education for the implementation of an international co-financed project. L. D. was supported by the Foundation for Polish Science within the project TEAM NET (POIR.04.04.00-00-16ED/18). A. S. O. and P. G. were supported by the Foundation for Polish Science within the project TEAM TECH (POIR.04.04.00-00-2159/16 00). A. S. O. acknowledges funding from the National Science Centre, Poland, within the project 2016/23/N/ST4/01020. J. G. was supported by the Foundation for Polish Science within the project First TEAM (POIR.04.04.00-00-26C7/16-00).

References

1 M. G. Santos, F. T. Bozza, M. Thomazini and C. S. Favaro-Trindade, *Food Chem.*, 2015, **171**, 32–39.
2 J. J. Liau, S. Hook, C. A. Prestidge and T. J. Barnes, *Eur. J. Pharm. Biopharm.*, 2015, **97**, 15–21.
3 C.-H. Choi, H. Wang, H. Lee, J. H. Kim, L. Zhang, A. Mao, D. J. Mooney and D. A. Weitz, *Lab Chip*, 2016, **16**, 1549–1555.
4 H. F. Chan, Y. Zhang and K. W. Leong, *Small*, 2016, **12**, 2720–2730.
5 M. Costantini, J. Guzowski, P. J. Żuk, P. Mozetic, S. De Panfilis, J. Jaroszewicz, M. Heljak, M. Massimi, M. Pierron, M. Trombetta, M. Dentini, W. Święszkowski, A. Rainer, P. Garstecki and A. Barbetta, *Adv. Funct. Mater.*, 2018, **28**, 1870133.
6 J. Guzowski, K. Gizynski, J. Gorecki and P. Garstecki, *Lab Chip*, 2016, **16**, 764–772.
7 G. Villar, A. D. Graham and H. Bayley, *Science*, 2013, **340**, 48–52.
8 E. Y. Liu, S. Jung, D. A. Weitz, H. Yi and C.-H. Choi, *Lab Chip*, 2018, **18**, 323–334.
9 B. Tal-Figiel, *Chem. Eng. Res. Des.*, 2007, **85**, 730–734.
10 G. Muschiolik and E. Dickinson, *Compr. Rev. Food Sci. Food Saf.*, 2017, **16**, 532–555.
11 J. Guzowski, S. Jakiela, P. M. Korczyk and P. Garstecki, *Lab Chip*, 2013, **13**, 4308.
12 F.-C. Chang and Y.-C. Su, *J. Micromech. Microeng.*, 2008, **18**, 065018.
13 M. Seo, C. Paquet, Z. Nie, S. Xu and E. Kumacheva, *Soft Matter*, 2007, **3**, 986.
14 A. R. Abate, A. T. Krummel, D. Lee, M. Marquez, C. Holtze and D. A. Weitz, *Lab Chip*, 2008, **8**, 2157.
15 J. Yan, W.-A. Bauer, M. Fischlechner, F. Hollfelder, C. Kaminski and W. Huck, *Micromachines*, 2013, **4**, 402–413.
16 A. Vian, B. Reuse and E. Amstad, *Lab Chip*, 2018, **18**, 1936–1942.
17 S. Okushima, T. Nisisako, T. Torii and T. Higuchi, *Langmuir*, 2004, **20**, 9905–9908.
18 T. Nisisako, S. Okushima and T. Torii, *Soft Matter*, 2005, **1**, 23.
19 A. S. Utada, E. Lorenceau, D. R. Link, P. D. Kaplan, H. A. Stone and D. A. Weitz, *Science*, 2005, **308**, 537–541.
20 L.-Y. Chu, A. Utada, R. Shah, J.-W. Kim and D. Weitz, *Angew. Chem.*, 2007, **119**, 9128–9132.
21 H. C. Shum, D. Lee, I. Yoon, T. Kodger and D. A. Weitz, *Langmuir*, 2008, **24**, 7651–7653.
22 D. Lee and D. A. Weitz, *Small*, 2009, **5**, 1932–1935.
23 S.-H. Kim, J. W. Kim, J.-C. Cho and D. A. Weitz, *Lab Chip*, 2011, **11**, 3162–3166.
24 H. C. Shum, Y.-j Zhao, S.-H. Kim and D. A. Weitz, *Angew. Chem., Int. Ed.*, 2011, **50**, 1648–1651.
25 B. Herranz-Blanco, E. Ginestar, H. Zhang, J. Hirvonen and H. A. Santos, *Int. J. Pharm.*, 2017, **516**, 100–105.
26 T. Nisisako, T. Ando and T. Hatsuzawa, *Lab Chip*, 2012, **12**, 3426.
27 M. B. Romanowsky, A. R. Abate, A. Rotem, C. Holtze and D. A. Weitz, *Lab Chip*, 2012, **12**, 802.
28 A. S. Opalski, K. Makuch, Y.-K. Lai, L. Derzsi and P. Garstecki, *Lab Chip*, 2019, **19**, 1183–1192.
29 F. Dutka, A. S. Opalski and P. Garstecki, *Lab Chip*, 2016, **16**, 2044–2049.
30 R. Dangla, E. Fradet, Y. Lopez and C. N. Baroud, *J. Phys. D: Appl. Phys.*, 2013, **46**, 114003.
31 S. Sugiura, M. Nakajima, S. Iwamoto and M. Seki, *Langmuir*, 2001, **17**, 5562–5566.
32 S. Sugiura, M. Nakajima and M. Seki, *Langmuir*, 2002, **18**, 5708–5712.
33 S. Sugiura, M. Nakajima, N. Kumazawa, S. Iwamoto and M. Seki, *J. Phys. Chem. B*, 2002, **106**, 9405–9409.
34 L. Shui, A. van den Berg and J. C. T. Eijkel, *Microfluid. Nanofluid.*, 2011, **11**, 87–92.

35 Z. Li, A. M. Leshansky, L. M. Pismen and P. Tabeling, *Lab Chip*, 2015, **15**, 1023–1031.
36 M. Hein, J.-B. Fleury and R. Seemann, *Soft Matter*, 2015, **11**, 5246–5252.
37 N. Mittal, C. Cohen, J. Bibette and N. Bremond, *Phys. Fluids*, 2014, **26**, 082109.
38 A. Montessori, M. Lauricella, E. Stolovicki, D. A. Weitz and S. Succi, *Phys. Fluids*, 2019, **31**, 021703.
39 A. Ofner, D. G. Moore, P. A. Rühs, P. Schwendimann, M. Eggersdorfer, E. Amstad, D. A. Weitz and A. R. Studart, *Macromol. Chem. Phys.*, 2017, **218**, 1600472.
40 S. Sahin and K. Schroën, *Lab Chip*, 2015, **15**, 2486–2495.
41 E. Crestel, L. Derzsi, H. Bartolomei, J. Bibette and N. Bremond, *Phys. Rev. Fluids*, 2019, **4**, 073602.
42 E. Stolovicki, R. Ziblat and D. A. Weitz, *Lab Chip*, 2018, **18**, 132–138.
43 Y.-T. Kao, T. S. Kaminski, W. Postek, J. Guzowski, K. Makuch, A. Ruszczak, F. von Stetten, R. Zengerle and P. Garstecki, *Lab Chip*, 2020, **20**, 54–63.
44 M. Schulz, S. Probst, S. Calabrese, A. R. Homann, N. Borst, M. Weiss, F. von Stetten, R. Zengerle and N. Paust, *Molecules*, 2020, **25**, 1914.
45 M. L. Eggersdorfer, W. Zheng, S. Nawar, C. Mercandetti, A. Ofner, I. Leibacher, S. Koehler and D. A. Weitz, *Lab Chip*, 2017, **17**, 936–942.
46 A. Ofner, I. Mattich, M. Hagander, A. Dutto, H. Seybold, P. A. Rühs and A. R. Studart, *Adv. Funct. Mater.*, 2019, **29**, 1806821.
47 S. Nawar, J. K. Stolaroff, C. Ye, H. Wu, D. T. Nguyen, F. Xin and D. A. Weitz, *Lab Chip*, 2020, **20**, 147–154.
48 N. Bremond, A. R. Thiam and J. Bibette, *Phys. Rev. Lett.*, 2008, **100**, 024501.
49 Z. Z. Chong, S. B. Tor, A. M. Gañán-Calvo, Z. J. Chong, N. H. Loh, N.-T. Nguyen and S. H. Tan, *Microfluid. Nanofluid.*, 2016, **20**, 66.
50 M. Bogdan, A. Montessori, A. Tiribocchi, F. Bonaccorso, M. Lauricella, L. Jurkiewicz, S. Succi and J. Guzowski, *Phys. Rev. Lett.*, 2022, **128**, 128001.
51 J. Guzowski and P. Garstecki, *Phys. Rev. Lett.*, 2015, **114**, 188302.
52 A. Montessori, M. Lauricella, S. Succi, E. Stolovicki and D. Weitz, *Phys. Rev. Fluids*, 2018, **3**, 072202.
53 A. R. Abate and D. A. Weitz, *Small*, 2009, **5**, 2030–2032.

